

# On Arrangement of Quadrics in Decomposing the Parameter Space of 3D Digitized Rigid Motions

Kacper Pluta · Guillaume Moroz · Yukiko Kenmochi · Pascal Romon

the date of receipt and acceptance should be inserted later

**Abstract** Comparing 3D shapes up to isometry is a classical geometric problem. In the case where voxels approximate the shapes, this requires to apply a 3D rigid motion on  $\mathbb{Z}^3$ . Unfortunately, such a motion does not preserve the topology of digital objects. Our main result is the decomposition of the 6D parameter space of digitized rigid motions for image patches of radius up to 3. Our approach reduces the problem to computing the arrangement of up to 741 quadrics – some of them being degenerate. State-of-the-art methods require a generic change of coordinates to handle the asymptotes, which makes our problem intractable. We address this issue by introducing and implementing a new algorithm for computing arrangement of quadrics in 3D, which handles degenerate directions and asymptotic critical values.

## 1 Introduction

Arrangements of algebraic varieties—e.g., surfaces given by second-degree polynomials—often appear as a critical element in studies where a problem (e.g., a search for possible non-conflicting movements of a robotic arm [19]) can be modeled as an enumeration of full-dimensional open cells bounded by surfaces in the respective parameter space. The final step then consists of reducing the allowed parameters’ set to only these open cells which fulfill the start assumptions

---

Kacper Pluta  
Technion – Israel Institute of Technology, Haifa, Israel

Guillaume Moroz  
Université de Lorraine, CNRS, Inria, LORIA, F-54000 Nancy

Yukiko Kenmochi  
LIGM, CNRS, Université Gustave Eiffel, F-77454, Marne-la-Vallée, France

Pascal Romon  
LAMA, Université Gustave Eiffel, Université Paris-Est Créteil, CNRS, F-77447, Marne-la-Vallée, France

e.g., a robotic arm does not hit any factory equipment or the arm does not perform a movement that could damage its servomotor.

At its core, this paper focuses on a problem of computing arrangement of hypersurfaces—in the 6D parameter space of 3D rigid motions—given by polynomials of degree two with integer coefficients. Our goal is then to enumerate 6-dimensional open cells bounded by these hypersurfaces.

Rigid motions defined on  $\mathbb{Z}^3$  are simple yet crucial operations in many digital image processing applications (e.g., image registration [41] and motion tracking [40]). However, it is also known that such operations cause geometric and topological defects [25, 26, 28, 29]. To address these issues, one can decompose the 6D parameter space of 3D rigid motions with respect to a digital shape, and then transform the shape by only these digitized rigid motions for which the parameters do not induce topological changes of the shape.

The state-of-the-art techniques such as cylindrical algebraic decomposition or critical point method [4] are respectively burdened—with respect to the number of variables—by double exponential [6] and exponential [34] complexities. Therefore, their direct applications to the problem of decomposing the six-dimensional parameter space of 3D digitized rigid motions are practically inefficient. Indeed, high dimensionality and the existence of degenerate cases such as asymptotic critical values [18]—e.g., a plane orthogonal to a coordinate axis is tangent to a hypersurface in a point at infinity—make a computation of such an arrangement difficult.

In this article, we propose an ad hoc method as follows. We first show that the problem of computing an arrangement of hypersurfaces in the 6D parameter space of 3D rigid motions can be simplified by uncoupling the six parameters of 3D rigid motions to end up with two systems in three variables, i.e., we obtain quadrics and planes in  $\mathbb{R}^3$ , which correspond to the rotational and translational parts of rigid motions,

respectively. We then, focus our study on computing sign vectors over the set of quadrics and show that the translational part of the original problem can be recovered from sample points of 3-dimensional open cells bounded by the quadrics. In our approach, we detect all topological changes along an arbitrary non-generic direction, and we compute all critical values including degenerate cases such as asymptotic critical values.

We note that our strategy for quadrics arrangement is similar to the one proposed by Mourrain et al. [22], and the main differences are: we do not use generic directions; we handle asymptotic cases and give new criteria to compute critical values in polynomials of degree two; we compute, and store at least one sample point for each full-dimensional open cell where Mourrain et al. [22] compute full adjacency information for all cells in an arrangement; moreover, we precompute all critical values a priori wherein the former approach only one type of critical values needs to be computed before the main algorithm. Finally, our implementation is provided together with some experiments for small digital objects.

In digital geometry and combinatorics, a few complexity analysis of problems similar to the one studied in this paper has been made for several geometric transformations. The complexities are related to the size of a given digital object in general:  $O(d^3)$  for 2D rotations [3];  $O(d^9)$  for 2D rigid motions [24] and  $O(d^{18})$  for 2D affine transformations [14], where  $d$  stands for a radius of a digital object. Later, in this article, we show that the theoretical complexity of such a problem for 3D rigid motions is  $O(d^{24})$ .

There are a few algorithms available for enumerating open cells in the parameter space of 2D rigid motions with respect to a digital object. Algorithms known to us are: 2D rotations [27]; 3D rotations around a given rational axis [38, 39]; 2D rigid motions [24, 31] and 2D affine transformations [14]. However, none of them handle the general case of 3D rigid motions that have 6 degrees of freedom.

This article is an extension of the conference paper [30]. Our new contributions compared to this preliminary work are: we determine the Euclidean type of the quadrics i.e., their types in  $\mathbb{R}^3$ , involved in the problem, and we show that they are smooth surfaces; we discuss the symmetric nature of the problem in the context of the proposed algorithm; we replace the calls to RAGlib [36] during the computation of an arrangement of conics with a recursive strategy of the main algorithm; finally, we briefly discuss the types of curves obtained from an intersection of two quadrics.

## 2 Classifying Rigid Motions of a 3D Digital Image

### 2.1 Rigid Motions on the 3D Cartesian Grid

Rigid motions on  $\mathbb{R}^3$  are bijective isometric maps defined as

$$\begin{cases} \mathcal{U} : \mathbb{R}^3 \rightarrow \mathbb{R}^3 \\ \mathbf{x} \mapsto \mathbf{Rx} + \mathbf{t} \end{cases} \quad (1)$$

where  $\mathbf{t} = (t_1, t_2, t_3) \in \mathbb{R}^3$  is a translation vector and  $\mathbf{R}$  is a rotation matrix. Let  $\mathbf{A}$  be the skew-symmetric matrix

$$\mathbf{A} = \begin{bmatrix} 0 & c & -b \\ -c & 0 & a \\ b & -a & 0 \end{bmatrix}$$

where  $a, b, c \in \mathbb{R}$ , and let  $\mathbf{I}$  be the  $3 \times 3$  identity matrix. Then almost any rotation matrix  $\mathbf{R}$  can be obtained via the Cayley transform [5]:

$$\begin{aligned} \mathbf{R} &= (\mathbf{I} - \mathbf{A})(\mathbf{I} + \mathbf{A})^{-1} \\ &= \frac{1}{d} \begin{bmatrix} 1 + a^2 - b^2 - c^2 & 2(ab - c) & 2(b + ac) \\ 2(ab + c) & 1 - a^2 + b^2 - c^2 & 2(bc - a) \\ 2(ac - b) & 2(a + bc) & 1 - a^2 - b^2 + c^2 \end{bmatrix}, \end{aligned} \quad (2)$$

where  $d = 1 + a^2 + b^2 + c^2$ . Indeed, rotations by  $\pi$  around any axis can only be obtained by the Cayley transform as a limit – angles of rotation converge to  $\pi$  when  $a, b, c$  tend to infinity [37]. In practice, this constraint is negligible and does not affect the generality of our study (see the following section which discusses the evolution of an image patch under 3D digitized rigid motions). Using this formula a rigid motion is parametrized by the six real parameters  $(a, b, c, t_1, t_2, t_3)$ .

According to Formula (1), we generally have  $\mathcal{U}(\mathbb{Z}^3) \not\subseteq \mathbb{Z}^3$ . As a consequence, in order to define digitized rigid motions as maps from  $\mathbb{Z}^3$  to  $\mathbb{Z}^3$ , we combine, as usual, the results of the rotation with a digitization operator that we define here as

$$\begin{cases} \mathcal{D} : \mathbb{R}^3 \rightarrow \mathbb{Z}^3 \\ (x_1, x_2, x_3) \mapsto \left( \lfloor x_1 + \frac{1}{2} \rfloor, \lfloor x_2 + \frac{1}{2} \rfloor, \lfloor x_3 + \frac{1}{2} \rfloor \right) \end{cases}$$

where  $\lfloor s \rfloor$  denotes the largest integer not greater than  $s$ , a digitized rigid motion is thus defined by  $U = \mathcal{D} \circ \mathcal{U}_{|\mathbb{Z}^3}$ . Due to the behavior of  $\mathcal{D}$  that maps  $\mathbb{R}^3$  onto  $\mathbb{Z}^3$ , digitized rigid motions are—most of the time—non-bijective. However, some are, and an algorithmic approach to verifying these digitized rotations is given in [32].

### 2.2 Image Patch and its Alterations under Digitized 3D Rigid Motions

Let us consider a finite set  $\mathcal{N}_r \subset \mathbb{Z}^3$ , called an *image patch*, whose center is  $\mathbf{c}$  and radius is  $r$  such that

$\mathcal{N}_r = \{\mathbf{v} \in \mathbb{Z}^3 \mid \|\mathbf{v} - \mathbf{c}\| \leq r\}$ . For simplicity we consider  $\mathbf{c}$  to be the origin. Next, we express the evolution of such an image patch  $\mathcal{N}_r$  under digitized rigid motions  $U$ .

The digitized rigid motions  $U = \mathcal{D} \circ \mathcal{U}$  are piecewise constant, and thus non-continuous, which is a consequence of the nature of the digitization operator  $\mathcal{D}$ . In particular, the image  $\mathcal{U}(\mathbf{v})$  of a point  $\mathbf{v} \in \mathbb{Z}^3$  may remain constant as the parameters of  $\mathcal{U}$  vary, and then suddenly jump from one point of  $\mathbb{Z}^3$  to another. In other words, an image patch  $\mathcal{N}_r$  evolves non-continuously, under digitized rigid motions, with respect to the parameters of  $\mathcal{U}$  that underlies  $U$  (see Figure 1). Hereafter, without loss of generality we assume that  $\mathcal{U}(\mathbf{c})$  stays in the digitization cell of  $\mathbf{c}$ , namely  $U(\mathbf{c}) = \mathbf{c}$ , since translation by an integer vector would not change the geometry of  $\mathcal{N}_r$ . Under this assumption we have that  $\mathbf{t} \in \left(-\frac{1}{2}, \frac{1}{2}\right)^3$ . Moreover, thanks to symmetry (reflections and rotations) we consider only non-negative  $a, b, c$ . Indeed, the rotation matrix  $\mathbf{R}$  obtained from Cayley transform for  $a, b, c$  corresponds to the rotation given by a quaternion  $\mathbf{q} = 1 + ai + bj + ck$ . Then let us consider rotations  $\sigma$  which are rotations by  $\frac{\pi}{2}k$ ,  $k \in \mathbb{Z}$ , around one of the main axes e.g.,  $\sigma : (x, y, z) \mapsto (-y, x, z)$ . Then, applying  $\sigma$  to  $\mathbf{q}$  we obtain  $\mathbf{q}' = 1 - bi + aj + ck$  and  $\sigma^{-1}$  maps  $\mathbf{q}'$  onto  $\mathbf{q}$ . We observe that, if  $a, b, c$  are negative then we can always find a series of  $\sigma$  rotations which map  $a, b, c$  to non-negative values and back.

Studying the non-continuous evolution of an image patch  $\mathcal{N}_r$  is equivalent to study the discontinuities of  $U(\mathbf{v})$  for every  $\mathbf{v} \in \mathcal{N}_r \setminus \{\mathbf{c}\}$ , which occur when  $\mathcal{U}(\mathbf{v})$  is on a *half-grid* plane, namely a boundary of a digitization cell. This is formulated by

$$\mathbf{R}_i \mathbf{v} + \mathbf{t}_i = k_i - \frac{1}{2} \quad (3)$$

where  $k_i \in H(\mathcal{N}_r) = \mathbb{Z} \cap [-r', r']$ ,  $\mathbf{R}_i$  is the  $i$ -th row of the rotation matrix for  $i \in \{1, 2, 3\}$  and  $r'$  is the longest radius of  $\mathcal{U}(\mathcal{N}_r)$  for all  $\mathcal{U}$ , so that  $r' = r + \sqrt{3}$ . We call the hypersurfaces of Equation (3) *tipping hypersurfaces*.

### 3 Arrangement of Quadrics

#### 3.1 The Problem as an Arrangement of Hypersurfaces

For any image patch  $\mathcal{N}_r$  the parameter space  $\Omega = \{(a, b, c, t_1, t_2, t_3) \in \mathbb{R}^6 \mid 0 \leq a, b, c, -\frac{1}{2} < t_i < \frac{1}{2}, i \in \{1, 2, 3\}\}$ , is partitioned by the set of tipping hypersurfaces, given by Equation (3), into a finite number of connected subsets – 6D open cells. The points in each cell induce different rigid motions  $\mathcal{U}_{|\mathcal{N}_r}$  but identical digitized rigid motions  $U_{|\mathcal{N}_r} = \mathcal{D} \circ \mathcal{U}_{|\mathcal{N}_r}$ .

**Remark 1** For a given image patch  $\mathcal{N}_r$ , tipping hypersurfaces (3) in  $\Omega$  are given by the possible combinations of integer 4-tuples  $(v_1, v_2, v_3, k_i)$  for  $i = 1, 2, 3$  where  $\mathbf{v} = (v_1, v_2, v_3) \in$

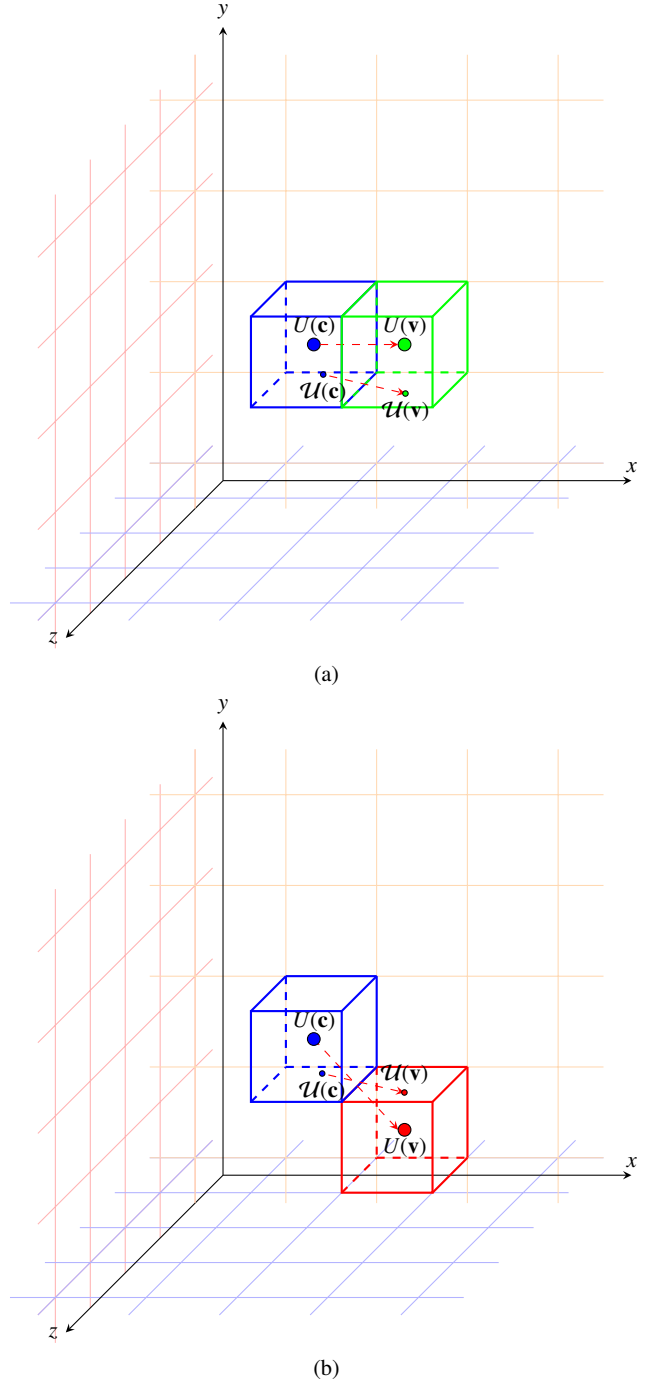


**Fig. 1** An example of discontinuity of  $U$ . In (a) and (b) the image  $\mathcal{U}(\mathbf{c})$  remains within the same unit cube—digitization cell—centered around the origin depicted in blue; thus the image  $U(\mathbf{c})$  is the same for the two digitized motions  $U$  associated to the continuous motions  $\mathcal{U}$  that slightly differ with respect to the parameters. However, the point  $\mathbf{v} = \mathbf{c} + (1, 0, 0)$ , has distinct images  $U(\mathbf{v})$  in (a) and (b); in (a), the digitization operator  $\mathcal{D}$  sends  $\mathcal{U}(\mathbf{v})$  onto the green integer point, while in (b), it sends  $\mathcal{U}(\mathbf{v})$  onto the red point

$\mathcal{N}_r \setminus \{\mathbf{c}\}$  and  $k_i \in H(\mathcal{N}_r)$ . Since  $|\mathcal{N}_r| - 1$  is in  $O(r^3)$  and  $|H(\mathcal{N}_r)|$  is in  $O(r)$ , the number of considerable tipping hypersurfaces is in  $O(r^4)$ , and thus in accordance with [12, Theorem

21.1.4] the overall complexity of the arrangement is theoretically bounded by  $O(r^{24})$ .

Our goal is to compute for each 6D open cell in  $\Omega$  at least one representative point called a *sample point*. As the direct application of cylindrical algebraic decomposition or critical points method to this problem is practically inefficient due to the high dimensionality and existence of degenerate cases that make the computation of the arrangement difficult. Hence, in the following discussion, we develop an indirect but still exact strategy.

### 3.2 Uncoupling the Parameters

The first idea of our strategy consists in uncoupling the parameters in the six-dimensional parameter space  $\Omega$ . Namely, we show that by considering the differences between the tipping hypersurfaces given in Equation (3) for different  $\mathbf{v} \in \mathcal{N}_r$  and  $\mathbf{k} \in H(\mathcal{N}_r)^3$ , we can reduce the problem to the study of an arrangement of surfaces in the  $(a, b, c)$ -space, and then lift the solution to the six-dimensional space.

Let us consider a rigid motion defined by  $\mathbf{R}$  and  $\mathbf{t}$ . The condition for having  $U(\mathbf{v}) = \mathbf{k} = (k_1, k_2, k_3) \in \mathbb{Z}^3$  where  $\mathbf{v} \in \mathcal{N}_r$  is

$$k_i - \frac{1}{2} < \mathbf{R}_i \mathbf{v} + t_i < k_i + \frac{1}{2}$$

for  $i = 1, 2, 3$ . Equivalently, we can write

$$k_i - \frac{1}{2} - \mathbf{R}_i \mathbf{v} < t_i < k_i + \frac{1}{2} - \mathbf{R}_i \mathbf{v}. \quad (4)$$

Then we call a *configuration* a list of couples  $(\mathbf{v}, \mathbf{k})$ , which describes how the image patch  $\mathcal{N}_r$  is transformed. This configuration can be described as a function

$$\begin{aligned} F : \mathcal{N}_r &\rightarrow H(\mathcal{N}_r)^3 \\ \mathbf{v} = (v_1, v_2, v_3) &\mapsto \mathbf{k} = (k_1, k_2, k_3). \end{aligned}$$

We would like to ascertain whether a given configuration  $F$  arises from a digitized rigid motion  $U$  i.e., it corresponds to some parameters  $a, b, c, t_1, t_2, t_3$ . Then the inequalities (4) state precisely the necessary and the sufficient conditions for the existence of the translation part  $\mathbf{t}$  of such a rigid motion, assuming that  $a, b, c$  are already known. Let us now remark that all these inequalities can be summed up in *three* inequalities indexed by  $i$ :

$$\max_{\mathbf{v} \in \mathcal{N}_r} \left( F(\mathbf{v})_i - \frac{1}{2} - \mathbf{R}_i \mathbf{v} \right) < \min_{\mathbf{v} \in \mathcal{N}_r} \left( F(\mathbf{v})_i + \frac{1}{2} - \mathbf{R}_i \mathbf{v} \right) \quad (5)$$

or, equivalently to the following list of inequalities

$$\forall \mathbf{v}, \mathbf{v}' \in \mathcal{N}_r, \quad F(\mathbf{v}')_i - \frac{1}{2} - \mathbf{R}_i \mathbf{v}' < F(\mathbf{v})_i + \frac{1}{2} - \mathbf{R}_i \mathbf{v}. \quad (6)$$

The key observation is that we have eliminated the variables  $t_1, t_2, t_3$  and have reduced the problem to a subsystem of inequalities in  $a, b, c$ .

Moreover, due to the rational expression in the Cayley transform (2), we may use the following polynomials of degree 2:

$$q_i[\mathbf{v}, k_i](a, b, c) = (1 + a^2 + b^2 + c^2)(2k_i - 1 - 2\mathbf{R}_i \mathbf{v}), \quad (7)$$

for  $i = 1, 2, 3$ , namely

$$\begin{aligned} q_1[\mathbf{v}, k_1](a, b, c) &= a^2(2(k_1 - v_1) - 1) + b^2(2(k_1 + v_1) - 1) \\ &\quad + c^2(2(k_1 + v_1) - 1) - 4a(bv_2 + cv_3) \\ &\quad - 4(bv_3 - cv_2) + 2(k_1 - v_1) - 1, \end{aligned}$$

$$\begin{aligned} q_2[\mathbf{v}, k_2](a, b, c) &= a^2(2(k_2 + v_2) - 1) + b^2(2(k_2 - v_2) - 1) \\ &\quad + c^2(2(k_2 + v_2) - 1) - 4b(av_1 + cv_3) \\ &\quad + 4(av_3 - cv_1) + 2(k_2 - v_2) - 1, \end{aligned}$$

$$\begin{aligned} q_3[\mathbf{v}, k_3](a, b, c) &= a^2(2(k_3 + v_3) - 1) + b^2(2(k_3 + v_3) - 1) \\ &\quad + c^2(2(k_3 - v_3) - 1) - 4c(av_1 + bv_2) \\ &\quad - 4(av_2 - bv_1) + 2(k_3 - v_3) - 1. \end{aligned}$$

Inequality (6) can be rewritten as the quadratic polynomial inequalities

$$\forall \mathbf{v}, \mathbf{v}' \in \mathcal{N}_r, Q_i[\mathbf{v}, \mathbf{v}', F(\mathbf{v})_i, F(\mathbf{v}')_i](a, b, c) > 0,$$

where

$$\begin{aligned} Q_i[\mathbf{v}, \mathbf{v}', k_i, k'_i](a, b, c) &= \frac{1}{2} q_i[\mathbf{v}, k_i](a, b, c) - \frac{1}{2} q_i[\mathbf{v}', k'_i](a, b, c) \\ &\quad + (1 + a^2 + b^2 + c^2), \end{aligned} \quad (8)$$

for  $i = 1, 2, 3$ , namely,

$$\begin{aligned} Q_1[\mathbf{v}, \mathbf{v}', k_1, k'_1](a, b, c) &= a^2(K_1 + V_1 + 1) + b^2(K_1 - V_1 + 1) \\ &\quad + c^2(K_1 - V_1 + 1) + 2a(cV_3 + bV_2) \\ &\quad + 2bV_3 - 2cV_2 + K_1 + V_1 + 1, \end{aligned} \quad (9)$$

$$\begin{aligned} Q_2[\mathbf{v}, \mathbf{v}', k_2, k'_2](a, b, c) &= a^2(K_2 - V_2 + 1) + b^2(K_2 + V_2 + 1) \\ &\quad + c^2(K_2 - V_2 + 1) + 2b(cV_3 + aV_1) \\ &\quad - 2aV_3 + 2cV_1 + K_2 + V_2 + 1, \end{aligned} \quad (10)$$

$$\begin{aligned} Q_3[\mathbf{v}, \mathbf{v}', k_3, k'_3](a, b, c) &= a^2(K_3 - V_3 + 1) + b^2(K_3 - V_3 + 1) \\ &\quad + c^2(K_3 + V_3 + 1) + 2c(bV_2 + aV_1) \\ &\quad + 2aV_2 - 2bV_1 + K_3 + V_3 + 1, \end{aligned} \quad (11)$$

where  $K_i = k_i - k'_i$ ,  $V_i = v'_i - v_i$ . The set of quadratic polynomials for our problem is then given by

$$= \{Q_i[\mathbf{v}, \mathbf{v}', k_i, k'_i](a, b, c) \mid i = 1, 2, 3, \mathbf{v}, \mathbf{v}' \in \mathcal{N}_r, k_i, k'_i \in H(\mathcal{N}_r)\}.$$

The zero sets of these polynomials are called *tipping quadrics*. Figure 2 illustrates some tipping quadrics.

### 4 Characterization of Tipping Quadrics

In this section, we provide a characterization of tipping quadrics.

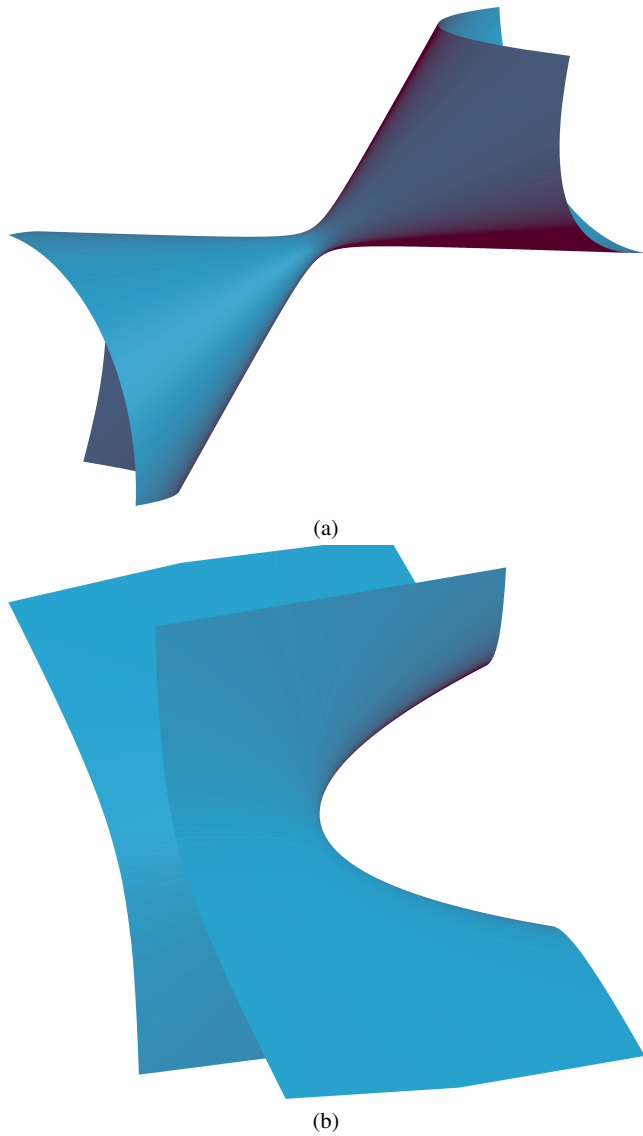


**Fig. 2** Examples of two types of the zero sets of quadratic polynomials of : (a) hyperboloid of one sheet and (b) hyperbolic paraboloid

#### 4.1 Symmetry

The symmetries of an image patch  $\mathcal{N}_r$  and the rotation matrix  $\mathbf{R}$  (see Equation (2)) are interesting from the computational point of view. Indeed, by applying the map  $\gamma : (a, b, c, v_1, v_2, v_3, k_i) \mapsto (b, c, a, v_2, v_3, v_1, k_{i \bmod 3+1})$  to the quadrics obtained from Equation (8) for a given  $i$  we can recover the whole set, e.g., an application of  $\gamma$  to Equation (9) yields quadrics of Equation (10).

Direct computations of tipping quadrics may induce non-real quadrics, e.g. an empty real set. Such non-real quadrics do not contribute to the problem of computing an arrangement of tipping quadrics, which are surfaces in  $\mathbb{R}^3$ , therefore, can be discarded. Also, thanks to the symmetry of tipping quadrics given by Equation (8) we can directly compute and discard

non-real quadrics only for one axis  $i$ , and then generate the other quadrics by applying the map  $\gamma$  to the valid quadrics obtained for the axis.

#### 4.2 Types of Tipping Quadrics

In this section we study the types of tipping quadrics  $Q(a, b, c) = 0$  for  $Q \in \mathbb{R}^{3 \times 3}$ . First we recall a classical result that a quadric  $q(a, b, c) = a^2A + b^2B + c^2C + 2bcD + 2acE + 2abF + 2aG + 2bH + 2cI + J = 0$ , is equivalently represented by a symmetric matrix

$$M_q = \begin{bmatrix} A & F & E & G \\ F & B & D & H \\ E & D & C & I \\ G & H & I & J \end{bmatrix}, \quad (12)$$

such that  $\mathbf{x}^t M_q \mathbf{x} = 0$ , where  $\mathbf{x}^t = (a, b, c, 1)$ . Also, the *inertia* of  $M_q$  is defined as a pair of  $(\sigma^+, \sigma^-)$ , where  $\sigma^+$  and  $\sigma^-$  denote the number of positive and negative eigenvalues of  $M_q$ , respectively. Then the type of a quadric  $q$  can be fully characterized by inertia of  $M_q$  and inertia of its left upper  $3 \times 3$  sub-matrix [8]. For a complete description of inertia based characterization we refer to [8, Table 1].

**Lemma 1** Any real quadric  $Q(a, b, c) = 0$  for  $Q \in \mathbb{R}^{3 \times 3}$ , has inertia  $(2, 2)$ .

*Proof* First, we notice that only quadrics of real types are relevant to our problem, in particular, the types of the inertias:  $(3, 1)$ ,  $(2, 2)$ ,  $(2, 1)$  and  $(1, 1)$  (see [8, Table 1]). Without loss of generality let us consider the case  $i = 1$ ,  $Q(a, b, c)$  is defined by Equation (9). This leads us to  $M_{Q(a,b,c)} =$

$$\begin{bmatrix} K_1 + V_1 + 1 & V_2 & V_3 & 0 \\ V_2 & K_1 - V_1 + 1 & 0 & V_3 \\ V_3 & 0 & K_1 - V_1 + 1 & -V_2 \\ 0 & V_3 & -V_2 & K_1 + V_1 + 1 \end{bmatrix}.$$

We then compute the eigenvalues of  $M_{Q(a,b,c)}$ , which are of the form  $1 + K_1 \pm \sqrt{V_1^2 + V_2^2 + V_3^2}$ , i.e. two are given as  $1 + K_1 + \sqrt{V_1^2 + V_2^2 + V_3^2}$  and the other two are given as  $1 + K_1 - \sqrt{V_1^2 + V_2^2 + V_3^2}$ . This leads us to a conclusion that if a quadric  $Q(a, b, c)$  is of a real type then the inertia of its symmetric matrix has to be  $(2, 2)$ .  $\square$

From Lemma 1 we have the following.

**Proposition 1** The quadrics given by the zero set of Equation (8) are either hyperboloids of one sheet or hyperbolic paraboloids.

Examples of quadrics given by the zero sets of Equation (8) are provided in Figure 2.

**Corollary 1** *The real quadrics  $Q(a, b, c) = 0$  for  $Q \in \mathcal{Q}$  are smooth.*

We do not prove Corollary 1 since it is known that quadrics of inertia  $(2, 2)$  are smooth [8].

## 5 Computing an Arrangement of Tipping Quadrics

In this section we discuss how to compute the arrangement of tipping quadrics  $Q(a, b, c) = 0$  for  $Q \in \mathcal{Q}$  given by Equation (8). Our strategy is similar to the one proposed by Mourrain et al. [22]. The main differences are that we do not store information about cells different from sample points of full-dimensional connected components; we precompute and sort all event points—points which induce changes of topology in an arrangement of quadrics—a priori. Moreover, we consider cases such as asymptotic critical values. In short, our method is as follows. Step 1: detect and sort all the events in which topology of the arrangement changes; Step 2: sweep by a plane the set of quadrics along a chosen direction. The sweeping plane stops between two event points, and we intersect quadrics related to them with the sweeping plane. For each of such points, this reduces to a problem of an arrangement of conics in 2D. After this procedure, for each sample point, we recover the translation part of the parameter space of digitized 3D rigid motions. The description of this last part will be given in the next section. Also, notice that proposed approach could be applied to solve a similar problem in 2D, i.e., generation of the different images of a 2D image patch under 2D digitized rigid motions – a solution to this problem was already proposed by Ngo et al. [24].

### 5.1 Bifurcation and Critical Values

In [22], the authors showed how to compute an arrangement of quadrics by sweeping a plane along a generic direction. Using the theory of *generalized critical values* [17, 18, 33] we show how to compute a point per open-connected component of an arrangement of quadrics using a projection along a non-generic direction – hereafter we consider the direction of the  $a$ -axis. Then by critical values, we denote values  $a$  at which the arrangement topology changes.

We consider an arrangement of smooth quadrics defined by zero sets of all respective polynomials in  $\mathbf{a}$ . In the following, for  $p, q, r \in I$ —where  $I$  is the index set of all polynomials in  $\mathbf{a}$ , which is finite for a given finite  $r$ —we denote by:  $S_p$  the surface given by  $Q_p(a, b, c) = 0$ ;  $C_{p,q}$  the curve defined by  $Q_p = Q_q = 0$  and  $P_{p,q,r}$  the points obtained as  $Q_p = Q_q = Q_r = 0$ . We assume that each  $C_{p,q}$  is a curve of dimension one that has either a finite number of singularities, or its projection is a point i.e.,  $C_{p,q}$  is a line.

Also, we denote by  $\mathcal{A}$  the set of maximally connected components of  $\mathbb{R}^3 \setminus \bigcup_p S_p$ .

Let  $C$  be an open cell of  $\mathcal{A}$ . We can associate to  $C$  the extremal values  $C_{\inf} = \inf(\{a \mid (a, b, c) \in C\})$  and  $C_{\sup} = \sup(\{a \mid (a, b, c) \in C\})$ . We will show in this section that these values are included in a bifurcation set. Furthermore, we consider that a projection map on the first coordinate  $a$  is denoted by  $\rho$ , and its restriction to a submanifold  $\mathcal{M} \subset \mathbb{R}^3$  is denoted by  $\rho|_{\mathcal{M}}$ . Moreover, for  $a_0 \in \mathbb{R}$  we denote by  $\mathcal{M}_{a_0}$  the set  $\rho_{|\mathcal{M}}^{-1}(a_0)$ . Similarly, for an open interval  $(a_0, a_1) \subset \mathbb{R}$  we denote by  $\mathcal{M}_{(a_0, a_1)}$  the set  $\rho_{|\mathcal{M}}^{-1}((a_0, a_1))$ .

We are interested in computing the set of values  $a$  above which the topology of the cells of  $\mathcal{A}$  changes. We show in Lemma 2 that this set is included in the finite bifurcation set [16] of the projections on the first axis restricted to different manifolds.

**Definition 1** Let  $\mathcal{M}$  be a submanifold of  $\mathbb{R}^3$ . Then a *bifurcation set* of  $\rho|_{\mathcal{M}}$  is the smallest set  $B(\rho|_{\mathcal{M}}) \subset \mathbb{R}$  such that  $\rho : \mathcal{M} \setminus \rho^{-1}(B(\rho|_{\mathcal{M}})) \rightarrow \mathbb{R} \setminus B(\rho|_{\mathcal{M}})$  is a locally trivial fibration (see Figure 3).

More specifically, for all  $a_0 \in \mathbb{R} \setminus B(\rho|_{\mathcal{M}})$ , there exists  $\epsilon > 0$  and a homeomorphism

$$\psi : (a_0 - \epsilon, a_0 + \epsilon) \times \mathcal{M}_{a_0} \rightarrow \mathcal{M}_{(a_0 - \epsilon, a_0 + \epsilon)},$$

such that  $\rho \circ \psi(x, \mathbf{p}) = x$  for all  $(x, \mathbf{p}) \in (a_0 - \epsilon, a_0 + \epsilon) \times \mathcal{M}_{a_0}$ . Figure 3 illustrates a 2D trivial and a 2D non-trivial fibrations.

In the following, we will consider the finite set  $B \subset \mathbb{R}$  defined as the union of the bifurcation sets of  $\rho|_{S_p}$  and  $\rho|_{C_{p,q}}$  and the projections of  $P_{p,q,r}$  [16]. More precisely, we define:

$$B_p = B(\rho|_{S_p}) \cup \bigcup_{q \neq p} B(\rho|_{C_{p,q}}) \cup \bigcup_{q \neq p, r \neq p, q \neq r} \rho(P_{p,q,r})$$

and  $B = \bigcup_p B_p$ . Then we state the following results that allow us to focus—during Step 2 of the algorithm—on a subset of quadrics of  $\mathcal{A}$ , i.e., a subset of quadrics which bound a maximal open-connected component.

**Lemma 2** *Let  $C$  be a maximal open-connected cell of  $\mathbb{R}^3 \setminus \bigcup_p S_p$ . Let  $\beta$  be the lowest value of  $B$  such that  $C_{\inf} < \beta$  and let  $v \in (C_{\inf}, \beta)$ . Finally, let  $\partial C_v$  be the boundary of  $C_v$  defined as an intersection of  $C$  with a plane  $a = v$ , and let  $J_C$  be a set of edges. More precisely,  $J_C$  is the set of indexes  $p$  such that the intersection of  $S_p$  with  $\partial C_v$  has dimension one. Then  $C_{\inf} \in B_p$  for all  $p \in J_C$ .*

*Proof* Let  $p \in J_C$  and let  $\mathbf{p}$  be a point on  $S_p \cap \partial C_v$  that does not belong to any surface  $S_q$  for  $q \neq p$ . Let  $\alpha \leq C_{\inf}$  be the maximal element of  $B_p$  lower than  $v$ . Then  $\rho|_{S_p}$  and the  $\rho|_{C_{p,q}}$  are trivial fibrations above  $(\alpha, \beta)$  and  $\rho(P_{p,q,r}) \cap (\alpha, \beta) = \emptyset$  for  $q \neq p$  and  $r \neq p$  different integers. In particular, the points of the curves  $C_{p,q}$  never cross above  $(\alpha, \beta)$ . More formally, there exists a continuous function  $\phi : (\alpha, \beta) \rightarrow S_p$  such that  $\phi(v) = \mathbf{p}$ ,  $\rho \circ \phi(x) = x$  and  $Q_q(\phi(x)) \neq 0$  for all  $q \neq p$ .

Let  $T_\epsilon$  be an open ball of radius  $\epsilon$  centered at  $\phi(v)$  and defined as  $T_\epsilon = \{\mathbf{y} = (a, b, c) \in \mathbb{R}^3 \mid v \in$

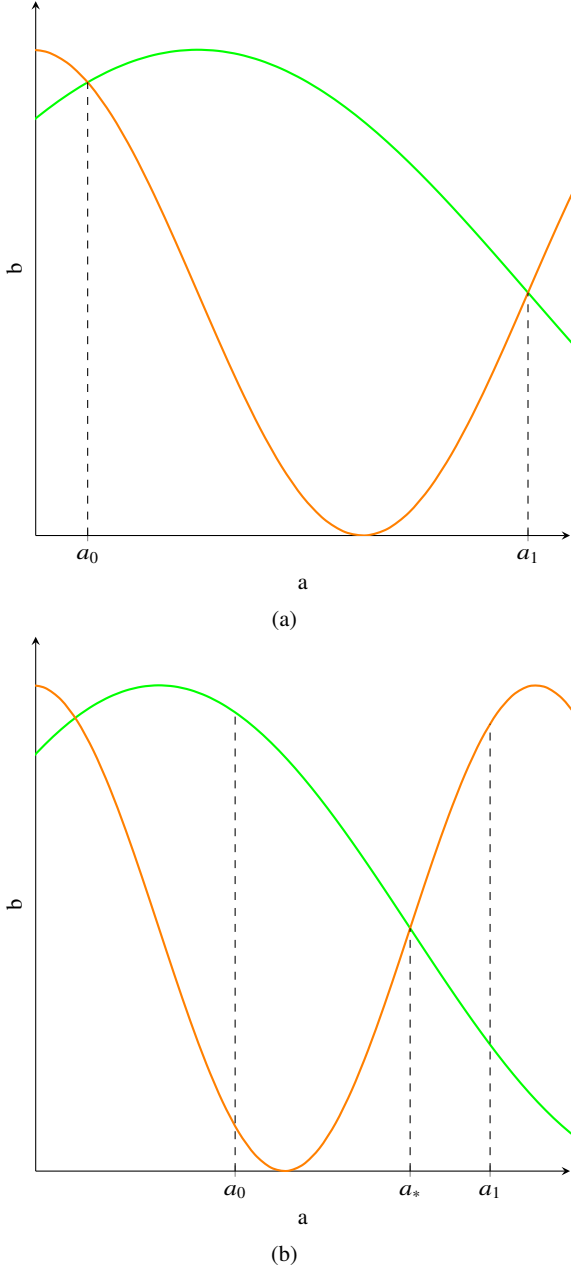


**Fig. 3** 2D examples demonstrating a locally trivial (a) and a non-trivial (b) fibrations. In (a), the topology of the arrangement above the open interval  $(a_0, a_1)$  is constant, while in (b) it is not, i.e. in (b) there is an element  $a_*$  of the bifurcation set  $B$  in the open interval  $(a_0, a_1)$ . Note that in (a)  $a_0, a_1 \in B$  while in (b)  $a_0, a_1 \notin B$ .

$[C_{\inf}, v]$  and  $\|(a, b, c) - \phi(v)\| < \epsilon\}$ . We now prove by contradiction that  $\alpha = C_{\inf}$ . If  $\alpha < C_{\inf}$ , then there exists a sufficiently small  $\epsilon > 0$  such that the respective intersections of  $T_\epsilon$  with  $Q_p < 0$  and  $Q_p > 0$  are connected and such that  $T_\epsilon$  does not intersect any  $S_q$  for  $q \neq p$ . Since  $p \in T_\epsilon$ , the intersection of  $T_\epsilon$  with  $C$  is not empty. Moreover,  $C$  is a maximally connected component in the complement of the union of  $S_j$ , such that one of the two connected components of  $T_\epsilon \setminus S_p$  is included in  $C$ . Thus, the ball  $T_\epsilon$  intersects  $C_a$

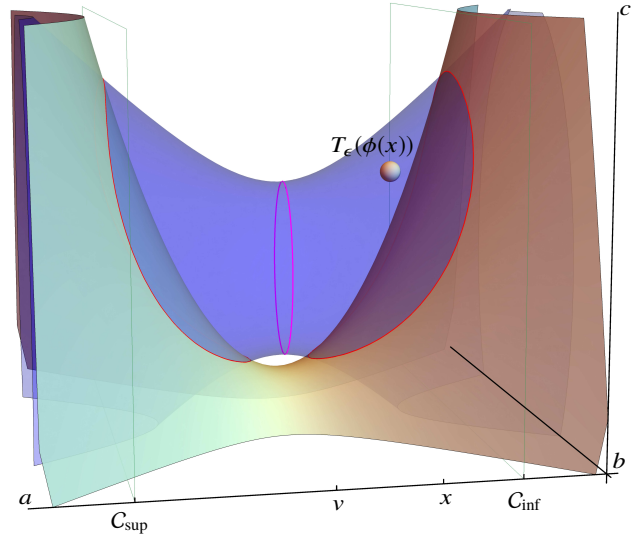


**Fig. 4** Visualization of a maximal connected component  $C$  bounded by two quadrics:  $Q_1 = ab + c$  (the green-orange surface) and  $Q_2 = a^2 + 4ab + b^2 + c^2 - 4c + 1$  (the blue surface). The two red curves represent the intersection of the surfaces i.e.,  $Q_1 = Q_2 = 0$ . The pink curve represents  $\partial C_v$ . The  $a$ -,  $b$ - and  $c$ -axes were re-oriented and the origin changed for a better visualization

for all  $a \in [C_{\inf}, v]$ . In particular,  $C_{C_{\inf}}$  is not empty, which is a contradiction with the definition of  $C_{\inf}$ . In particular,  $C_{\inf} = \alpha$ , which allows us to conclude that  $\alpha = C_{\inf}$  and  $C_{\inf} \in B_p$ .  $\square$

Figure 4 shows a maximal connected component  $C$  bounded by two quadrics, and Figure 3(a) illustrates intervals such that the topology of some  $C_a$ ,  $a \in (\alpha, \beta)$ , remains constant.

For each value  $u \in B$ , we denote by  $J_u \subset I$  the set of indexes  $p$  such that  $u \in B_p$ . Moreover, for a set of indexes  $J_u$ , we denote by  $\mathcal{A}_{J_u}$  the set of maximally open-connected components of  $\mathbb{R}^3 \setminus \bigcup_{j \in J_u} S_j$ .

**Corollary 2** Let  $C$  be a maximal open-connected cell of  $\mathbb{R}^3 \setminus \bigcup_p S_p$ . Let  $m > C_{\inf}$  be the smallest value of  $B$  greater than  $C_{\inf}$ . For all  $a \in (C_{\inf}, m)$ , there exists a cell  $C' \in \mathcal{A}_{J_{C_{\inf}}}$  such that  $C'_a \subset C_a$ .

*Proof* According to Lemma 2,  $C_{\inf}$  is contained in all  $B_p$  such that  $S_p$  contains a subset of dimension one of the border of  $C_a$ . In particular, one of the cells of  $\mathcal{A}_{J_{C_{\inf}}} \cap \rho^{-1}(a)$  is included in  $C_a$ .  $\square$

From a constructive point of view, the authors of [17] showed that the bifurcation set is included in the union of the critical and asymptotic critical values. More specifically, given a polynomial map  $f : M \rightarrow \mathbb{R}$ , we have  $B(f) \subset K(f) \cup K_\infty(f)$ , where  $K(f)$  are the critical values of  $f$  and  $K_\infty$  are its asymptotic critical values. In [22], the authors called the points of  $K(\rho|_{S_p})$  events of type A, the points of  $K(\rho|_{C_{p,q}})$  events of type B and the points  $\rho(P_{p,q,r})$  events of type C.

We extend their classification for degenerate projections, and say that the points of  $K_\infty(\rho|_{S_p})$  are events of type  $A_\infty$  and the points of  $K_\infty(\rho|_{C_{p,q}})$  are events of type  $B_\infty$ .

From a computational point of view, we recall in the next section how to compute the critical values of types A, B and C. For the types  $A_\infty$  and  $B_\infty$ , we use the results from [17] and simplify them for the case of quadrics.

Finally, as described in Section 5.5, our strategy will be to compute the generalized critical values  $a$ , and for each such a value to store  $J_a$  – the set of indexes, such that either:

- $a \in K(\rho|_{S_p}) \cup K_\infty(\rho|_{S_p})$
- $a \in K(\rho|_{C_{p,q}}) \cup K_\infty(\rho|_{C_{p,q}})$  for  $q \neq p$
- $a \in \rho(P_{p,q,r})$  for  $q \neq p, r \neq p$  and  $q \neq r$

This approach allows us to reduce the number of quadrics that are necessary to consider in the intermediate steps of our sweeping plane algorithm.

## 5.2 Detection of Critical Values

In this section we show how to compute the critical values of types A, B and C. Finally, for the types  $A_\infty$  and  $B_\infty$ , we use the results from [17] and simplify them for the case of quadrics.

**Type A.** The first type corresponds to values  $s \in K(\rho|_{S_p})$  above which the topology of open-connected components in  $\mathcal{A}$  changes. Algebraically, such an event corresponds to a value  $s \in \mathbb{R}$  for which there is a solution to the system  $Q_p(s, b, c) = \partial_b Q_p(s, b, c) = \partial_c Q_p(s, b, c) = 0$ , for  $p \in I$  and  $s$  is called  $a$ -critical value. In other words, this corresponds to the situation  $a = s$  is tangent to a quadric  $Q_p(a, b, c) = 0$ .

**Type B.** This type corresponds to the case  $s \in K(\rho|_{C_{p,q}})$ . Such an event corresponds to an  $s$ -value for which there are solutions to the system  $Q_p(s, b, c) = Q_q(s, b, c) = (\nabla Q_p \times \nabla Q_q)_1(s, b, c) = 0$ , where  $p, q \in I$  and  $p \neq q$ . In other words, either the curve defined by  $Q_p(s, b, c) = Q_q(s, b, c) = 0$ , is tangent to a plane orthogonal to the  $a$ -axis or a point  $(s, b, c)$  is a singularity point of the curve  $C_{p,q}$ .

Note that, the values of type B include projections of the isolated singularities, i.e., two quadrics intersect in a point or a line that projects on a point.

**Type C.** There are values  $s \in \rho(P_{p,q,r})$  above which the topology of the open-connected components in  $\mathcal{A}$  changes. An  $a$ -critical value is such that there are solutions to the system  $Q_p(s, b, c) = Q_q(s, b, c) = Q_r(s, b, c) = 0$ , where  $p, q, r \in I$  and  $p \neq q, q \neq r, r \neq p$ . In other words, the quadrics intersect in a point. Note that an intersection between three quadrics can be a curve. This issue can be solved if a curve projects on a point, thanks to the elimination theory and use of resultants or Gröbner basis. Indeed, we can compute a

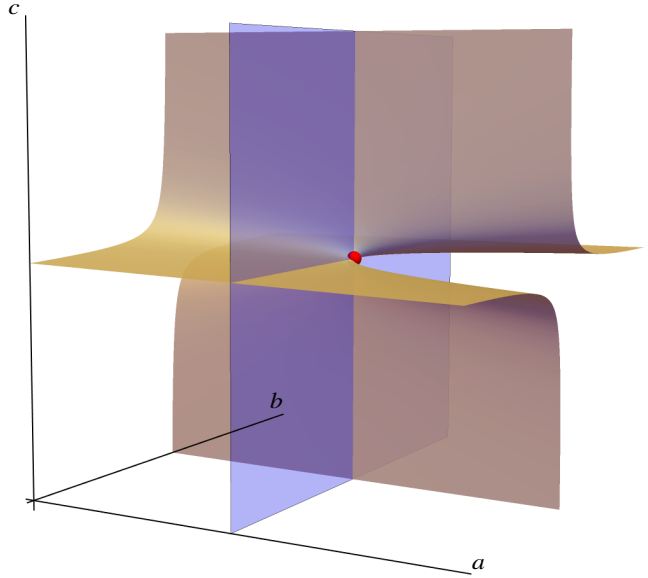


**Fig. 5** Example of an event of type A – a sweeping plane  $a = 0$  (depicted in violet) tangent at a point (depicted in red) to a quadric  $Q = bc - a = 0$ . Note that, the origin has been changed for a better visualization

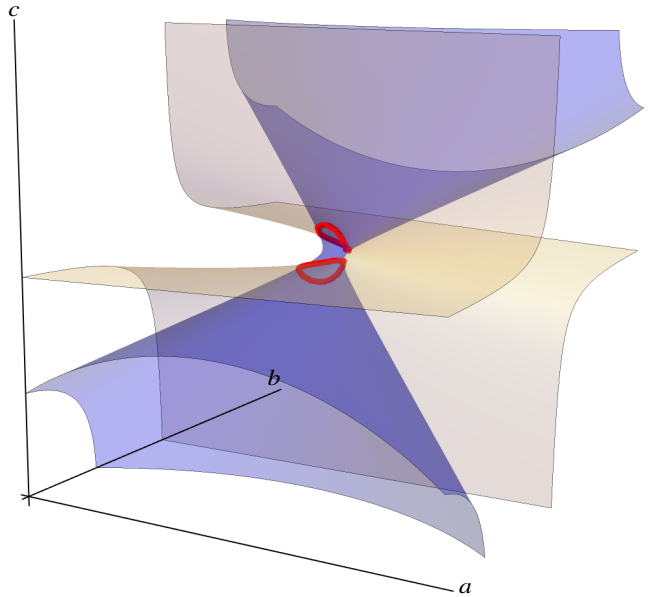


**Fig. 6** Example of an event of type B – a sweeping plane is tangent to two curves (depicted in red) given by an intersection of quadrics  $Q_1 = bc + a = 0$  and  $Q_2 = a^2 + b^2 - 4bc + c^2 + 4a + 1 = 0$ . Note that, the origin has been changed for a better visualization

univariate polynomial which vanishes on the projection of the curve [7].

For more information about events of the types A, B and C we refer readers to [22]. Figures 5-7 show examples of events of the types A, B and C.

Right now, we are going to discuss the cases of asymptotic critical values.

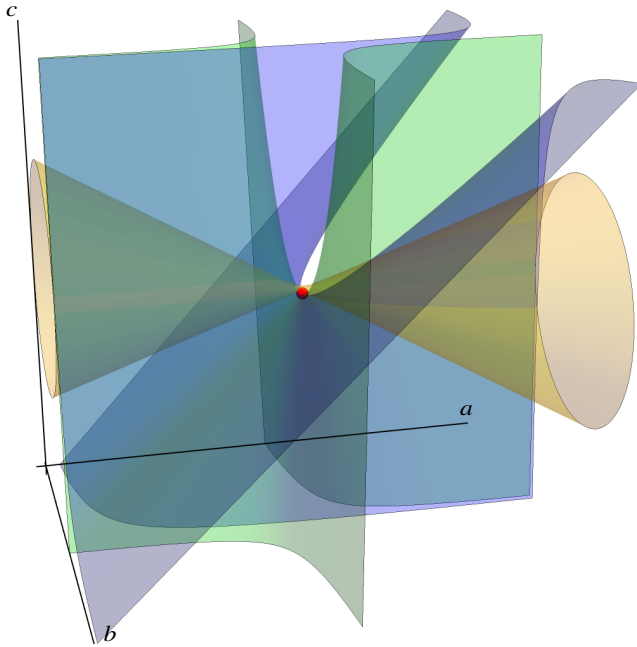


**Fig. 7** Example of an event of type C – a point (depicted in red) given by an intersection of quadrics  $Q_1 = ab - c = 0$ ,  $Q_2 = ab - ac - b - c = 0$  and  $Q_3 = a^2 - ab + c^2 - c = 0$ . Note that, the origin has been changed for a better visualization

**Type  $A_\infty$ .** This type of critical values corresponds to the situation when a plane orthogonal to one of the coordinate axes is tangent to a quadric at a point at infinity (see Figure 8).

**Lemma 3** Let  $S$  be a smooth quadric defined by  $Q(a, b, c) = 0$ . Denoting by  $M(a)$  the matrix  $\begin{pmatrix} \frac{\partial^2 Q}{\partial b^2} & \frac{\partial^2 Q}{\partial b \partial c} & \frac{\partial Q}{\partial b}(a, 0, 0) \\ \frac{\partial^2 Q}{\partial c \partial b} & \frac{\partial^2 Q}{\partial c^2} & \frac{\partial Q}{\partial c}(a, 0, 0) \end{pmatrix}$  that depends only on  $a$ ,

$$K_\infty(\rho|_S) \subset \{a \mid M(a) \text{ has rank at most 1}\}.$$

**Proof** Consider the mapping  $f : \mathbb{R}^3 \rightarrow \mathbb{R}^2$  such that  $(a, b, c) \mapsto (a, Q(a, b, c))$ . The definition of  $K_\infty$  implies  $K_\infty(\rho|_S) = K_\infty(f) \cap \mathbb{R} \times \{0\}$ . Let  $f(a, b, c) = \frac{\max(|\frac{\partial Q}{\partial b}|, |\frac{\partial Q}{\partial c}|)}{\max(|\frac{\partial Q}{\partial a}|, |\frac{\partial Q}{\partial b}|, |\frac{\partial Q}{\partial c}|)}$ . Then using [17, Proposition 2.5 and Definition 3.1] with  $df = \begin{pmatrix} 1 & 0 & 0 \\ \frac{\partial Q}{\partial a} & \frac{\partial Q}{\partial b} & \frac{\partial Q}{\partial c} \end{pmatrix}$ , there exists a sequence

$(a_n, b_n, c_n) \in \mathbb{R}^3$  such that  $|b_n| + |c_n| \rightarrow \infty$  and  $a_n \rightarrow a$  and  $(|b_n| + |c_n|)f(a_n, b_n, c_n) \rightarrow 0$ . In particular, since  $\frac{\partial Q}{\partial a}$ ,  $\frac{\partial Q}{\partial b}$  and  $\frac{\partial Q}{\partial c}$  are linear functions, this implies that in the definition of  $K_\infty$ , the expression  $|b_n| + |c_n|$  divided by the denominator of  $f(a_n, b_n, c_n)$  is bounded. In particular the numerator of  $f(a_n, b_n, c_n)$  converges toward 0. More specifically,  $\frac{\partial Q}{\partial b}$  and  $\frac{\partial Q}{\partial c}$  converge toward 0. On the other hand, either  $|b_n|$  or  $|c_n|$  goes toward infinity. Assume without restriction of generality that  $|b_n|$  goes toward infinity. In this case, the

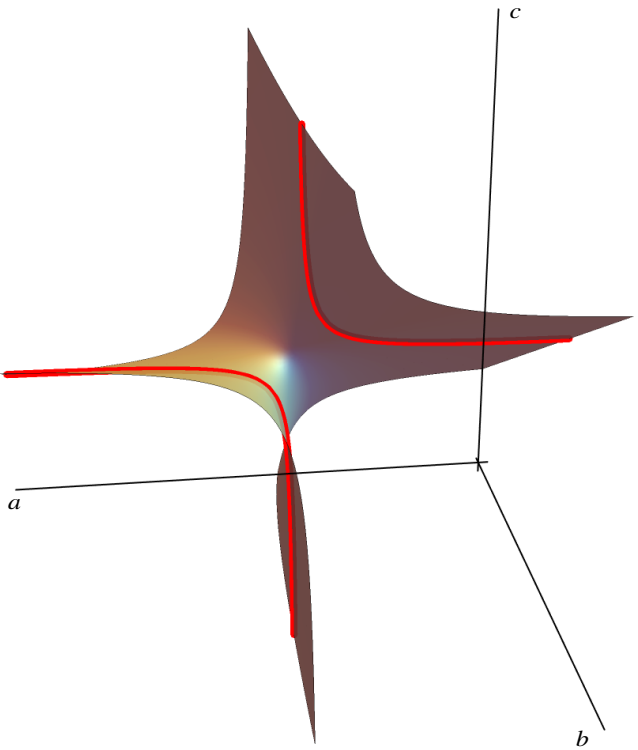


**Fig. 8** Example of asymptotic critical value. There exist a plane  $a = 0$  tangent to an asymptote—the red curves in the surface  $Q = ab - 2ac - 2b - c = 0$ —in a point at infinity. Note that the origin has been moved for a better visualization

function  $\frac{\partial^2 Q}{\partial c^2} \frac{\partial Q}{\partial b} - \frac{\partial^2 Q}{\partial b \partial c} \frac{\partial Q}{\partial c}$  is a linear function that depends only on  $b$ . Then this function converges toward 0 if and only if the coefficient in front of  $b$  in the function and its constant coefficient are 0. In particular, from the minor-rank relation and the symmetry of the second order partial derivatives we have that if  $\frac{\partial^2 Q}{\partial c^2}$  or  $\frac{\partial^2 Q}{\partial b \partial c}$  is non-zero, the matrix  $M(a)$  has rank 1. If both are 0, then with similar arguments, we can see that  $M(a)$  is the null matrix. Thus,  $K_\infty$  is a subset of  $a$  such that  $M(a)$  has a rank less than or equal to 1.  $\square$

The algorithm to detect this type of events of tipping quadrics is as follows. Step 1: we compute  $\partial_b Q(a, b, c) = ub + vc + wa + t$  and  $\partial_c Q(a, b, c) = u'b + v'c + w'a + t'$ , where  $u, v, w, t, u', v', w', t' \in \mathbb{Z}$  are coefficients of the corresponding polynomials and  $Q \in \mathcal{P}$ . Step 2: let  $\mathbf{v}$  stands for the cross product of  $\mathbf{v}_b = (u, v, wa + t)$  and  $\mathbf{v}_c = (u', v', w'a + t')$ . Note that the vectors  $\mathbf{v}_b$  and  $\mathbf{v}_c$  represent the rows of  $M(a)$ . Finally, we solve for  $a$  such that all the elements of  $\mathbf{v}$  are equal to 0, i.e. all the second minors of  $M(a)$  are equal to 0, in other words when the rank of  $M(a)$  is lower than 2.

**Type  $B_\infty$ .** In this case we are considering the asymptotic critical points of the projection restricted to a curve defined by the intersection of two quadrics  $Q_p = 0, Q_q = 0 \in \mathcal{P}, p, q \in I$  and  $p \neq q$ . Using [17, Proposition 4.2], these correspond to the  $a$ -coordinate of the sweeping planes that cross the

projective closure of the curve at infinity. More formally, we have:  $K_\infty(\rho|_{C_{p,q}}) = \{a \mid \exists(a_n, b_n, c_n) \in C_{p,q} \text{ such that } |b_n| + |c_n| \rightarrow +\infty \text{ and } a_n \rightarrow a\}$ . In particular, this set is also the set of values  $a$  such that either the projection of  $C_{p,q}$  on the  $(a, b)$ -plane or the projection of  $C_{p,q}$  on the  $(a, c)$ -plane has an asymptote in  $a$ .

According to [17, Proposition 4.2], these are the elements of a non-properness set of a projection map. More formally, we say that  $\mathbf{p}$  belongs to a non-properness set of a projection map  $\pi$  if for each neighborhood  $Y$  of  $\mathbf{p}$  we have that  $\pi^{-1}(Y)$  is not bounded. The properties of this set and the algorithms to compute it have been studied notably in [11, 15, 21]. In our case the non-properness set of the projection restricted to  $C_{p,q}$  is the set of  $a$ -coordinates of the sweeping planes that cross at infinity the projective closure of  $C_{p,q}$ , i.e., the smallest projective algebraic variety containing  $C_{p,q}$ .

To detect such a case we apply the following steps. Step 1: we project the curve  $C_{p,q}$  to the  $(a, b)$ -plane (resp.  $(a, c)$ -plane) eliminating the  $c$  (resp.  $b$ ) variable, and denote the corresponding polynomials as  $P_b(a, b)$  (resp.  $P_c(a, c)$ ). Step 2: let  $C_b(a)$  and  $C_c(a)$  stand for head coefficients—coefficients of leading monomials—of  $P_b(a, b)$  and  $P_c(a, c)$ , respectively. The asymptotic critical value for a pair of quadrics happens for  $C_b(a) = 0$  or  $C_c(a) = 0$ . For instance, let us consider the polynomial  $(2a - 1)c^2 + a^2$ . Then, the leading coefficient is  $2a - 1$  and when  $a = \frac{1}{2}$  we have that  $c$  can take any value. Indeed, there is an asymptote for  $a = \frac{1}{2}$ . Figure 9 illustrates an event of  $B_\infty$  type and Figure 10 the corresponding projections.

### 5.3 Symmetry of B and C Type Events

The computations of the B and C type events are the most expensive. Indeed, if computed directly, the corresponding complexities are, respectively,  $O(n^2)$  and  $O(n^3)$  where  $n$  is the number of quadrics (see Equation 8). Perhaps, the complexity of this step could be reduced by an observation that if three quadrics intersect at  $a = s$  then the other three quadrics obtain from them by applying the maps  $\phi : (a, b, c) \mapsto (a, -c, b)$  and  $\xi : (a, b, c) \mapsto (-a, b, c)$  also intersect at  $a = s$  or  $a = -s$ . Figure 11 provides a visualization of the maps' actions on quadrics.

**Proposition 2** Let  $Q_s \subset$  stands for a doublet (resp. triplet) of quadrics that induce a B (resp. C) type event at  $a = s$ . Then,  $\phi : (a, b, c) \mapsto (a, -c, b)$  and  $\xi : (a, b, c) \mapsto (-a, b, c)$  applied to  $Q_s$  induces another doublet (resp. triplet) of quadrics that also induce an event at  $a = s$  (or  $a = -s$ ).

*Proof* From the matrix representation of Quadratic Normal Form (see Matrix (12)) it can be verified that  $\phi$  (resp.  $\xi$ ) applied to a quadric  $Q_1$  given by Equation (9) does not change the shape of the corresponding matrix, i.e., the positions of zeros, but the signs and the placement of the coefficients. Since

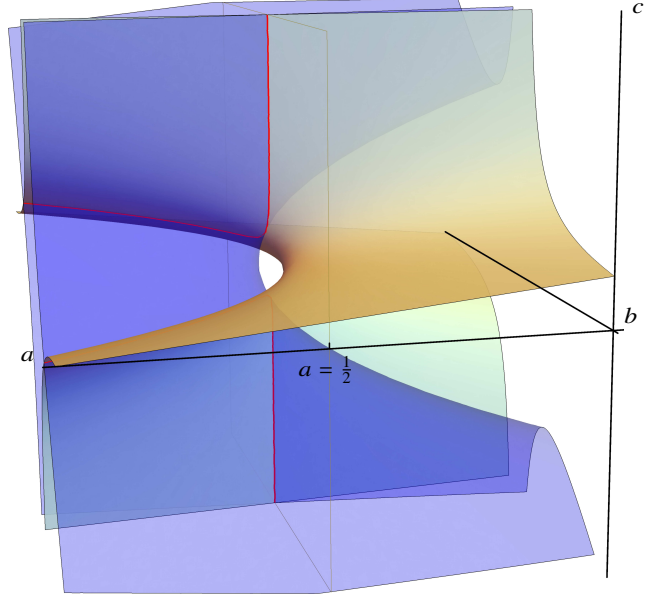


**Fig. 9** Visualization of a critical event of  $B_\infty$  type. The intersection of quadrics:  $Q_1 = bc + a = 0$  (the orange-green surface) and  $Q_2 = b^2 - bc + a - 1 = 0$  (the blue surface) leads to the red curves which exhibit an asymptotic behavior at  $a = \frac{1}{2}$ . The  $a$ -,  $b$ - and  $c$ - axes are re-oriented and the origin is changed for a better visualization effect. The respective projections of  $C_{1,2}$  onto the  $(a, b)$ - and  $(a, c)$ -plane are illustrated in Figure 10

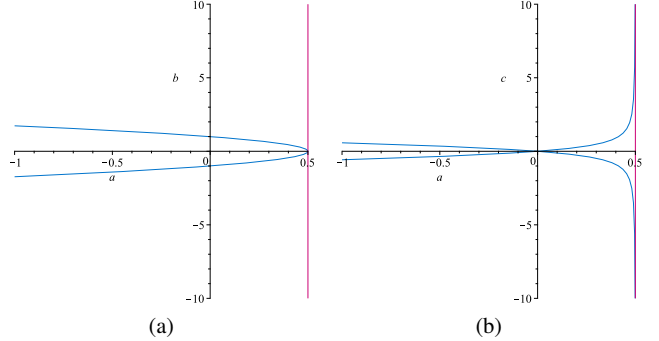


**Fig. 10** Visualization of the projections of  $C_{p,q}$  (the light blue curve) defined by the same quadrics as in Figure 9. These projections are  $P_b(a, b) = b^2 + 2a - 1$ , (a) and  $P_c(a, c) = 2ac^2 + a^2 - c^2$ , (b). We have an asymptote in the  $(a, c)$ -plane for  $2a - 1 = 0$ , i.e. when  $a = \frac{1}{2}$ —which is marked by a pink vertical line.

the coefficients are symmetric  $\phi(Q_1) \in$  (resp.  $\xi(Q_1) \in$ ). Using the same argument about symmetricity the coefficients one can show that in the case of a quadric  $Q_2$  given by Equation (10) (resp.  $Q_3$  given by Equation (11)) the corresponding matrix of Quadratic Normal Form is transformed under  $\phi$  (resp.  $\xi$ ) to a matrix corresponding to a quadric given by Equation (11) and vice versa.

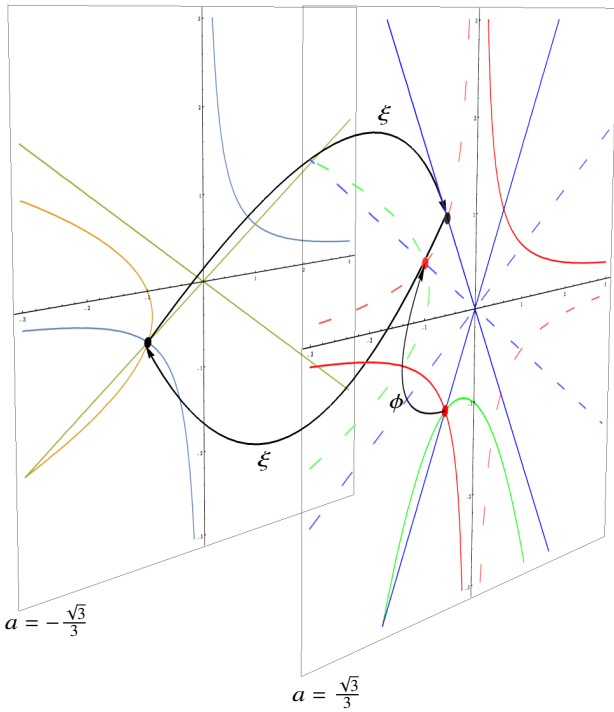


**Fig. 11** Visualization of the actions of  $\phi$  and  $\xi$  on a set of the quadrics. On the one hand, in the plane  $a = \frac{\sqrt{3}}{3}$  there is a C type event (represented by a red point) given by an intersection of  $Q_1 = a - cb$ ,  $Q_2 = ab + b^2 + c + 1$  and  $Q_3 = 3a^2 + 3b^2 - c^2 - 1$  (the red, green and blue curves) that are mapped under  $\phi$  to  $Q'_1 = a + cb$ ,  $Q'_2 = -ac + c^2 + b + 1$  and  $Q'_3 = 3a^2 - b^2 + 3c^2 - 1$  (the dashed red, green and blue curves) that also induce a C type event (the red point pointed by the arrow) in  $a = \frac{\sqrt{3}}{3}$ . An application of  $\phi$  can be seen as a rotation in the plane  $a = \frac{\sqrt{3}}{3}$ . On the other hand,  $\xi$  maps the three quadrics that intersects at  $a = -\frac{\sqrt{3}}{3}$  (the black point) to a triple of the quadrics that intersects at  $a = \frac{\sqrt{3}}{3}$  (the black point) and vice versa. The action of  $\xi$  on the quadrics can be seen as a reflection. Note that in the case of the map  $\xi$  the mapping to the plane  $a = \frac{\sqrt{3}}{3}$  is represented only by the black points

Then, the matrix forms of  $\phi$  and  $\xi$  are

$$\begin{bmatrix} 1 & 0 & 0 \\ 0 & 0 & -1 \\ 0 & 1 & 0 \end{bmatrix} \quad \text{and} \quad \begin{bmatrix} -1 & 0 & 0 \\ 0 & 0 & 1 \\ 0 & 1 & 0 \end{bmatrix},$$

which are rotation matrices corresponding to rotations by an angle  $\theta = \frac{\pi}{2}$  around  $\omega = (1, 0, 0)$ , and by an angle  $\theta = \pi$  around  $\omega = (0, \frac{1}{\sqrt{2}}, \frac{1}{\sqrt{2}})$ , respectively.

From this we conclude that applications of  $\phi$  and  $\xi$  to the quadrics  $Q_s \subset \mathcal{C}$  gives a set of quadrics that also induce an event at  $a = s$  or  $a = -s$ .  $\square$

We note that an open question is how to exploit the symmetries and the maps  $\gamma$ ,  $\phi$ , and  $\xi$  to obtain an efficient implementation of an algorithm computing the B and C type events.

#### 5.4 Sorting Critical Values

In this section, we focus on the representation of  $a$ -critical values as real algebraic numbers—roots of univariate polynomials—and operations such as comparisons of them, which are necessary to sort  $a$ -critical values.

Similarly to Mourrain et al. [22], we represent a real algebraic number  $\alpha$  as a pair: an irreducible univariate polynomial  $P \in \mathbb{Z}[a]$  such that  $P(\alpha) = 0$  and an open isolating interval  $(g, h)$ , with  $g, h \in \mathbb{Q}$ , containing  $\alpha$  and such that there is no other root of  $P$  in this interval. Note that the isolation of the roots of an irreducible univariate polynomial can be made using Descartes' rule [35].

Let  $\alpha = (P, (g, h))$  and  $\beta = (Q, (i, j))$  such that  $P, Q \in \mathbb{Z}[a]$  and  $g, h, i, j \in \mathbb{Q}$ , stand for two real algebraic numbers. Then we can conclude if  $\alpha = \beta$  while checking a sign of  $\gcd$  – a polynomial greatest common divisors of  $P$  and  $Q$  at an intersecting interval. Note that, when  $\gcd(P, Q)$  is a polynomial then its roots are the common roots of  $P$  and  $Q$ . On the other hand, to conclude if  $\alpha$  is greater than  $\beta$  or  $\beta$  greater than  $\alpha$ , we apply a strategy which consists of refining the isolating intervals until they are disjoint. When two intervals are disjoint then we can compare their bounds and conclude if  $\alpha$  is greater than  $\beta$  (or  $\beta$  greater than  $\alpha$ )<sup>1</sup>. To refine an isolating interval of real roots, one can use e.g., bisection of intervals, Newton interval method [13], [23, Chapter 5] or quadratic interval refinement method proposed by Abbot [2].

The ability to compare two different algebraic numbers allows us to sort a list of events which can be done with well-known sorting algorithms such as quicksort.

#### 5.5 Sweeping a Set of Quadrics

After sorting the set of  $a$ -critical values we are ready to compute sample points of open cells. The sweeping plane moves along the  $a$ -axis and stops between two consecutive  $a$ -critical values in a *midpoint*. At such a midpoint, the sweeping plane intersects the set of quadrics. On this plane orthogonal to the  $a$ -axis, the subproblem becomes the arrangement of conics, which can be solved by applying a strategy similar to the one developed for the main problem. More precisely, we compute and sort a set of  $b$ -critical values (or  $c$ -critical values) in the arrangement of conics and sweep it by a line. Figure 12 shows conics for three  $a$ -critical values in an arrangement of two quadrics.

The remaining question is which quadrics we should use at each midpoint to avoid missing an open cell. In our approach, we use all the quadrics of for the first midpoint (see Figure 13). Then for any other midpoint, we use only the

<sup>1</sup> Our implementation of real algebraic numbers and their comparison can be downloaded from <https://github.com/copyme/RigidMotionsMapleTools>

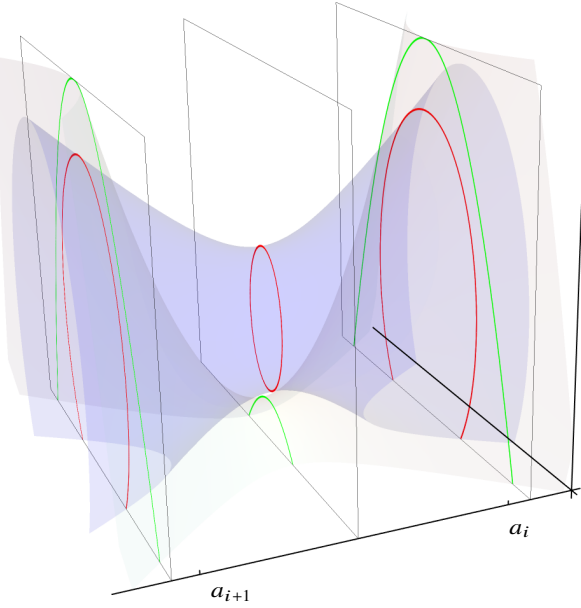


**Fig. 12** Visualization of sweeping of a set of the quadrics (see Figure 4). Intersection planes at three different points. Between the planes we have  $a$ -critical values ( $a_i$  and  $a_{i+1}$ ) –  $a$  values in which topology of an arrangement changes. Conics obtain from quadrics in red and green

quadrics related to the lowermost critical value from the pair of  $a$ -critical values that bound this midpoint. Indeed, doing so we ensure that at the end of our strategy we collect at least one sample point for each full-dimensional open cell thanks to Lemma 2, Corollary 2 and Lemma 3.

## 6 Recovering Translation Parameter Values

The algorithm proposed in the previous section gives us the set  $\mathcal{R}$  of sample points  $(a, b, c) \in \mathbb{Q}^3$ , which correspond to the rotation parameters. In this section we discuss how to obtain sample points  $(t_1, t_2, t_3)$  of the translation part for each  $(a, b, c) \in \mathcal{R}$  and how to generate different images of an image patch under rigid motions.

Let us first note that Equation (3) under the assumption of  $\mathbf{t} \in \left(-\frac{1}{2}, \frac{1}{2}\right)^3$  defines the set of planes in the range  $= \left(-\frac{1}{2}, \frac{1}{2}\right)^3$  for each  $(a, b, c) \in \mathcal{R}$ , by setting  $\mathbf{v} \in \mathcal{N}$  and  $\mathbf{k} \in H(\mathcal{N})^3$ . These planes divide into cuboidal regions. Figure 14 illustrates an example of such critical planes in .

To obtain different images of an image patch  $\mathcal{N}$  rotated by a given  $a, b, c \in \mathbb{Q}$ , under translations  $(t_1, t_2, t_3) \in$ , we compute the arrangement of planes in which involves sorting of critical planes and finding a midpoint of each cuboidal region bounded by them.

**Remark 2** Note that we can have several sample points  $(a, b, c)$  inducing the topologically equivalent arrangement of planes (the order of planes is identical). Therefore, to avoid unnecessary calculations we can define a hash function  $\mathcal{H}$

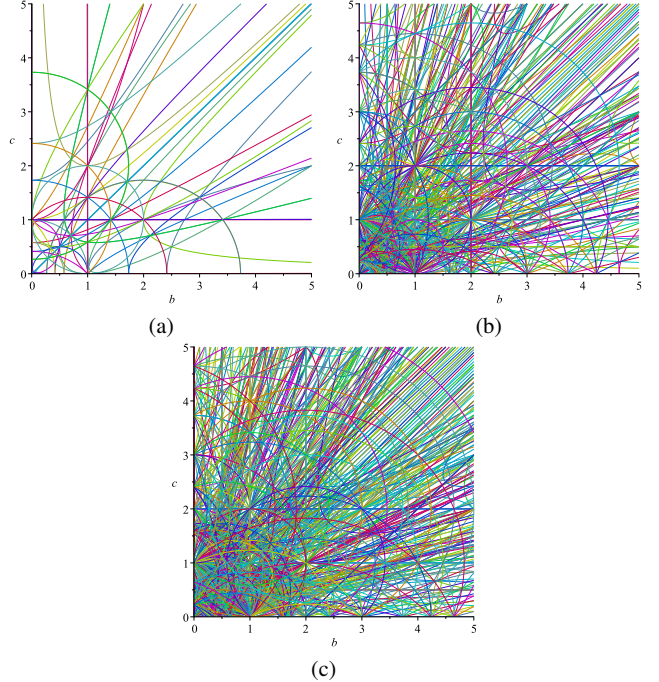


**Fig. 13** The first intersections of 81, 513 and 741 quadrics obtained for  $\mathcal{N}_1$ ,  $\mathcal{N}_2$  and  $\mathcal{N}_3$ , respectively

which returns a different signature for each sample point  $(a, b, c)$  which induce a different order of the critical planes.

To define a hash function  $\mathcal{H}$ , let  $\mathcal{I}$  stands for a collection of indexes of critical planes. Then we define the hash function

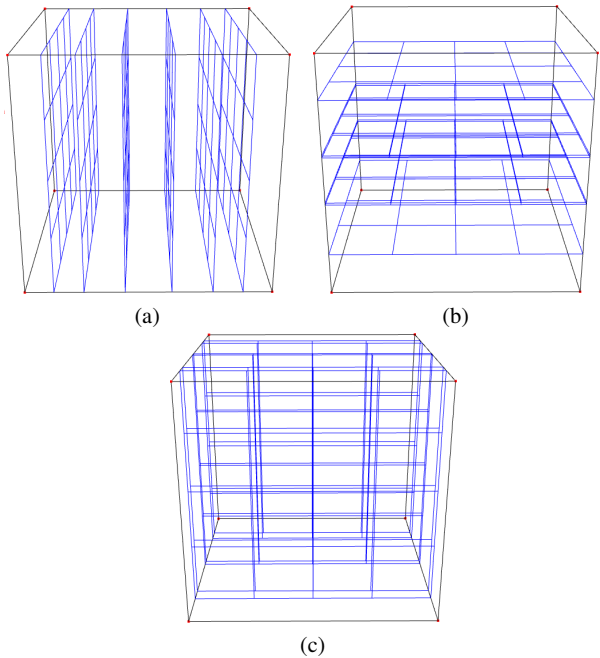


**Fig. 14** Visualization of the critical planes for  $\mathcal{N} = \{(1, 0, 0), (0, 1, 0), (0, 0, 0), (-1, 0, 0), (0, -1, 0), (0, 0, -1)\}$  and some  $(a, b, c)$ . For the sake of visibility three types of orthogonal critical planes are presented separately

that returns the sorted indices of  $\mathcal{I}$  with respect to the order of critical planes.

**Remark 3** We also note that, as  $(a, b, c)$  change between cells possible not cells changes their topology in the  $(t_1, t_2, t_3)$ -space. This observation tells us that some image patches will not vary between different cells in  $(a, b, c)$ -space. To avoid having duplicated image patches, we simple perform—as a post-processing step—a direct comparison of the obtained image patches and keep only unique ones together with the corresponding parameters  $(a, b, c, t_1, t_2, t_3)$ .

## 7 Experimental Results

In this section, we discuss some characteristics of the arrangement that we discuss with respect to a given image patch.

### 7.1 Combinatorial Aspects of Quadrics

The number of quadrics obtained directly from Equation (8) for  $\mathcal{N}_r(\mathbf{p})$ ,  $r = 1, 2, 3$  is 1260, 26790 and 106596, respectively. In this section we show that this number for  $\mathcal{N}_1(\mathbf{p})$  is reduced to 81 by discarding those which are always strictly positive (resp. negative) and ones which are redundant. Note that similar studies remain valid for different image patches. Indeed, the numbers of quadrics after the reduction for  $\mathcal{N}_2(\mathbf{p})$  and  $\mathcal{N}_3(\mathbf{p})$  are 513 and 741, respectively<sup>2</sup>.

Let us consider  $\mathcal{N}_1(\mathbf{p})$  and vectors  $\mathbf{u}_1 = (1, 0, 0)$  (resp.  $\mathbf{u}_2 = (0, 1, 0)$ ,  $\mathbf{u}_3 = (0, 0, 1)$ ), and  $\mathbf{h} = \left(\frac{1}{2}, \frac{1}{2}, \frac{1}{2}\right)$ . Then we rewrite (6) as

$$\mathbf{u}_i \cdot (\mathbf{k}' - \mathbf{h} - \mathbf{R}\mathbf{v}') < \mathbf{u}_i \cdot (\mathbf{k} + \mathbf{h} - \mathbf{R}\mathbf{v}) \quad (13)$$

for  $i = 1, 2, 3$  where  $\mathbf{v}, \mathbf{v}' \in \mathcal{N}_1(\mathbf{p})$ ,  $\mathbf{k}, \mathbf{k}' \in H(\mathcal{N}_1(\mathbf{p}))^3$ . This induces

$$k_i - k'_i + 1 - \mathbf{u}_i \cdot \mathbf{R}(\mathbf{v} - \mathbf{v}') > 0, \quad (14)$$

where we know that  $q = k_i - k'_i + 1 \in \mathbb{Z} \cap [-1, 3]$ . We then consider the following different cases of  $v = \|\mathbf{v} - \mathbf{v}'\|$ , and we consider  $k$  and  $k'$  such that for any  $\mathbf{R}$  Equation 14 is valid.

1. when  $v = 0$ , then there is no  $q \in \mathbb{Z} \cap [-1, 3]$  satisfying (14),
2. when  $v = 1$ , then there are 6 different pairs of  $(\mathbf{v}, \mathbf{v}')$  and we obtain  $q \in \{0\}$ ,
3. when  $v = 2$ , then there are 6 different pairs of  $(\mathbf{v}, \mathbf{v}')$  and we obtain  $q \in \{-1, 0, 1\}$ ,
4. when  $v = \sqrt{2}$ , then there are 12 different pairs of  $(\mathbf{v}, \mathbf{v}')$  and we obtain  $q \in \{-1, 0, 1\}$ .

<sup>2</sup> The complete list of the polynomials can be downloaded from <https://doi.org/10.5281/zenodo.839212>

Therefore, the number of valid quadrics  $Q[\mathbf{v}, \mathbf{v}', k_i, k'_i]$  for each case is 0 (case 1), 6 (case 2), 18 (case 3) and 36 (case 4). Note that case 2 is included in case 3 up to a constant, so we can ignore the 6 quadrics. This finally gives us  $\frac{18+36}{2} = 27$  quadrics per direction and thus 81 in total.

### 7.2 Intersection of Two Quadrics

In Table 1 we provided curves' types that are given as an intersection of two quadrics (B type events) for  $\mathcal{N}_3(\mathbf{0})$ . Note that, from all the types in Table 1 only smooth quartics are not singular [10]. More information about the types of intersection and visualizations of them can be found in [9].

Type in the real projective space $\mathbb{P}^3(\mathbb{R})$	Number of cases
smooth quartic, two finite components	67540
smooth quartic, one finite component	63916
smooth quartic, two infinite components	26548
two lines	7460
cubic and secant line	2868
nodal quartic, affinely finite	1956
two secant conics, affinely finite	1070
double line	965
skew quadrilateral	828
nodal quartic, affinely infinite	658
point	552

**Table 1** Types of intersections computed with *QI* (version 1.0.1) [1, 20] for the quadrics obtained for  $\mathcal{N}_3(\mathbf{0})$

### 7.3 Computing Sample Points

Having implemented the algorithm we have used it to compute sample points for image patches of different sizes, i.e.,  $\mathcal{N}_i$ ,  $i = 1, 2, 3$ . Due to technical issues—we used different machines or even a cluster of six machines—we cannot provide exact computation times. Nevertheless, say that they very from a few—for  $\mathcal{N}_1$ —to several days—for  $\mathcal{N}_3$ .

One of the rather clear drawbacks of our algorithm is that it generates a lot of redundant sample points. Indeed, even for  $\mathcal{N}_3$  we have obtained several dozens of gigabytes of data, which is a drawback of the proposed method.

## 8 Conclusions

In this article, we proposed a method to decompose the 6D parameter space of digitized rigid motions for a given 3D

image patch. We first uncouple the six parameters of 3D rigid motions to end up with two systems in three variables and start by studying an arrangement of quadrics in  $\mathbb{R}^3$ .

Our approach to computing an arrangement of quadrics in 3D is similar to the one proposed by Mourrain et al. [22] where the main differences are; we do not use generic directions; we handle asymptotic cases and give new criteria to compute critical values in polynomials of degree two; we compute, and store at least one sample point for each full-dimensional open cell where Mourrain et al. [22] compute full adjacency information for all cells in an arrangement. Moreover, we precompute all critical values a priori wherein the former approach only one type of critical values needs to be computed before the main algorithm. Those sample points are then used to decompose the other three-dimensional parameter space. We also provided our implementation together with experiment estimations for some small image patch.

As a part of our future work, we would like to use the presented method in a study of topological alteration of  $\mathbb{Z}^3$  under 3D digitized rigid motions.

## Acknowledgement

The authors express their thanks to David Cœurjolly of CNRS, Université de Lyon, (France) for running some computations on the CC-IN2P3 cluster in Lyon. Also, we thank Sylvain Lazard of Inria Nancy (France) for his very helpful feedback and comments which allowed us to improve the article.

## References

1. QI: Quadric Intersection, <http://vegas.loria.fr/qi/>
2. Abbott, J.: Quadratic Interval Refinement for Real Roots. *Communications in Computer Algebra* 48(1/187), 3–12 (2014)
3. Amir, A., Kapah, O., Tsur, D.: Faster two-dimensional pattern matching with rotations. *Theoretical Computer Science* 368(3), 196–204 (2006)
4. Basu, S., Pollack, R., Roy, M.F.: Algorithms in real algebraic geometry. Springer Berlin Heidelberg (2005)
5. Cayley, A., Forsyth, A.: The Collected Mathematical Papers of Arthur Cayley, vol. 1. The University Press (1898)
6. Collins, G.: Quantifier elimination for real closed fields by cylindrical algebraic decomposition. In: Automata Theory and Formal Languages. LNCS, vol. 33, pp. 134–183. Springer Vienna (1975)
7. Cox, D., Little, J., O’Shea, D.: Ideals, Varieties and Algorithms. An Introduction to Computational Algebraic Geometry and Commutative Algebra. Springer-Verlag New York (1996)
8. Dupont, L., Lazard, D., Lazard, S., Petitjean, S.: Near-optimal parameterization of the intersection of quadrics: I. The generic algorithm. *Journal of Symbolic Computation* 43(3), 168–191 (2008)
9. Dupont, L., Lazard, D., Lazard, S., Petitjean, S.: Near-optimal Parameterization of the Intersection of Quadrics: II. A Classification of Pencils. *Journal of Symbolic Computation* 43(3), 192–215 (2008)
10. Dupont, L., Lazard, D., Lazard, S., Petitjean, S.: Near-Optimal Parameterization of the Intersection of Quadrics: III. Parameterizing Singular Intersections. *Journal of Symbolic Computation* 43(3), 216–232 (2008)
11. El Din, M.S., Schost, É.: Properness Defects of Projections and Computation of at Least One Point in Each Connected Component of a Real Algebraic Set. *Discrete & Computational Geometry* 32(3), 417 (2004)
12. Halperin, D.: Arrangements. In: Goodman, J.E., O’Rourke, J. (eds.) *Handbook of Discrete and Computational Geometry*, 2nd Ed., pp. 529–562. Chapman and Hall/CRC (2004)
13. Hansen, E.: Global optimization using interval analysis – the multi-dimensional case. *Numerische Mathematik* 34(3), 247–270 (1980)
14. Hundt, C., Liskiewicz, M.: On the Complexity of Affine Image Matching. In: STACS. Lecture Notes in Computer Science, vol. 4393, pp. 284–295. Springer Berlin Heidelberg (2007)
15. Jelonek, Z.: Topological characterization of finite mappings. *Bull. Polish Acad. Sci. Math* 49(3), 279–283 (2001)
16. Jelonek, Z., Kurdyka, K.: On Asymptotic Critical Values of a Complex Polynomial. *Journal für die reine und angewandte Mathematik* 2003(565), 1–11 (2003)
17. Jelonek, Z., Kurdyka, K.: Quantitative generalized Bertini-Sard theorem for smooth affine varieties. *Discrete & Computational Geometry* 34(4), 659–678 (2005)
18. Kurdyka, K., Orro, P., Simon, S., et al.: Semialgebraic Sard theorem for generalized critical values. *Journal of differential geometry* 56(1), 67–92 (2000)
19. Latombe, J.C.: Robot motion planning, vol. 124. Springer Science & Business Media (2012)
20. Lazard, S., Peñaranda, L.M., Petitjean, S.: Intersecting Quadrics: An Efficient and Exact Implementation. *Computational Geometry* 35(1), 74–99 (2006)
21. Moroz, G.: Properness defects of projection and minimal discriminant variety. *Journal of Symbolic Computation* 46(10), 1139–1157 (2011)
22. Mourrain, B., Tecourt, J.P., Teillaud, M.: On the computation of an arrangement of quadrics in 3D. *Computational Geometry* 30(2), 145–164 (2005)
23. Neumaier, A.: Interval Methods for Systems of Equations. *Encyclopedia of Mathematics and its Applications*, Cambridge University Press Cambridge (1991)
24. Ngo, P., Kenmochi, Y., Passat, N., Talbot, H.: Combinatorial structure of rigid transformations in 2D digital images. *Computer Vision and Image Understanding* 117(4), 393–408 (2013)
25. Ngo, P., Kenmochi, Y., Passat, N., Talbot, H.: Topology-preserving conditions for 2D digital images under rigid transformations. *Journal of Mathematical Imaging and Vision* 49(2), 418–433 (2014)
26. Ngo, P., Passat, N., Kenmochi, Y., Talbot, H.: Topology-preserving rigid transformation of 2D digital images. *IEEE Transactions on Image Processing* 23(2), 885–897 (2014)
27. Nouvel, B., Rémy, E.: Configurations induced by discrete rotations: Periodicity and quasi-periodicity properties. *Discrete Applied Mathematics* 147(2–3), 325–343 (2005)
28. Passat, N., Kenmochi, Y., Ngo, P., Pluta, K.: Rigid motions in the cubic grid: A discussion on topological issues. In: Discrete Geometry for Computer Imagery (DGCI). Lecture Notes in Computer Science, vol. 11414. Springer, Marne-la-Vallée, France (2019), <https://hal.archives-ouvertes.fr/hal-01892944>
29. Pluta, K., Kenmochi, Y., Passat, N., Talbot, H., Romon, P.: Topological alterations of 3D digital images under rigid transformations. Research report, Université Paris-Est, Laboratoire d’Informatique Gaspard-Monge UMR 8049 (2014), <https://hal.archives-ouvertes.fr/hal-01333586>
30. Pluta, K., Moroz, G., Kenmochi, Y., Romon, P.: Quadric Arrangement in Classifying Rigid Motions of a 3D Digital Image. In: CASC. Lecture Notes in Computer Science, vol. 9890, pp. 426–443. Springer (2016)
31. Pluta, K., Romon, P., Kenmochi, Y., Passat, N.: Bijective rigid motions of the 2D Cartesian grid. In: DGCI. pp. 359–371. Lecture Notes in Computer Science, Springer (2016)

32. Pluta, K., Romon, P., Kenmochi, Y., Passat, N.: Bijectivity Certification of 3D Digitized Rotations. In: CTIC. Lecture Notes in Computer Science, vol. 9667, pp. 30–41. Springer International Publishing Switzerland (2016)
33. Rabier, P.J.: Ehresmann fibrations and Palais-Smale conditions for morphisms of Finsler manifolds. Annals of Mathematics pp. 647–691 (1997)
34. Renegar, J.: On the computational complexity and geometry of the first-order theory of the reals. Part I: Introduction. Preliminaries. The geometry of semi-algebraic sets. The decision problem for the existential theory of the reals. Journal of symbolic computation 13(3), 255–299 (1992)
35. Rouillier, F., Zimmermann, P.: Efficient isolation of polynomial's real roots . Journal of Computational and Applied Mathematics 162(1), 33–50 (2004)
36. Safey El Din, M.: Testing Sign Conditions on a Multivariate Polynomial and Applications. Mathematics in Computer Science 1(1), 177–207 (2007)
37. Singla, P., Junkins, J.L.: Multi-resolution methods for modeling and control of dynamical systems. CRC Press Boca Raton (2008)
38. Thibault, Y.: Rotations in 2D and 3D discrete spaces. Ph.D. thesis, Université Paris-Est (2010)
39. Thibault, Y., Sugimoto, A., Kenmochi, Y.: 3D discrete rotations using hinge angles. Theoretical Computer Science 412(15), 1378–1391 (2011)
40. Yilmaz, A., Javed, O., Shah, M.: Object tracking: A survey. Acm computing surveys (CSUR) 38(4), 13 (2006)
41. Zitova, B., Flusser, J.: Image registration methods: a survey. Image and vision computing 21(11), 977–1000 (2003)